Hall Thruster Krypton Sputtering Effects on Vacuum Facility Materials

IEPC-2024-549

Presented at the 38th International Electric Propulsion Conference
Pierre Baudis Convention Center • Toulouse, France
June 23-28, 2024

Ryan W. Cowan[1], Saptarshi Biswas[2], Luke K. Franz[3], Christopher M. Cretel[4], Richard A. Obenchain[5]
Oregon State University, Corvallis, OR, 97330, USA

and

Richard E. Wirz[6]
Oregon State University, Corvallis, OR, 97331, USA
University of California, Los Angeles, CA, 90095, USA

Electric propulsion (EP) ground tests need to address multiple facility effects such as carbon sputtering, erosion, and deposition across the inner surfaces of both the thruster and vacuum chamber facilities. As part of a multi-university experimental investigation of the H9 Hall effect thruster as a part of JANUS (Joint Advanced Propulsion Institute), this paper reports on surface morphology of polycrystalline graphite with different grain sizes and stainless-steel 304 panels tested based on the total time integrated flux of incident ions produced by the thruster. Erosion and deposition observations are discussed with regard to their locations within the facility and expected ion flux from the plume. Scanning Electron Microscope (SEM) images provide useful qualitative surface morphology. Preliminary optical profilometry and laser confocal methods provide quantitative results but with high uncertainty due to the short test duration and surface anomalies; but inform improved approaches to future tests. Preliminary Energy-dispersive X-ray spectroscopy (EDS) measurements reveal evidence of stainless-steel and aluminum sputtered material. These results support companion sputter/deposition modeling efforts and suggest that additional graphite shielding of facility surfaces and use of optimized volumetrically complex materials (VCMs) may prove beneficial.

[1] Graduate Research Assistant, Oregon State University, cowanry@oregonstate.edu
[2] Post-doctorate research faculty, Oregon State University, saptarshi.biswas@oregonstate.edu
[3] Graduate Research Assistant, Oregon State University, and franzlu@oregonstate.edu
[4] Graduate Research Assistant, Oregon State University, cretelch@oregonstate.edu
[5] Graduate Research Assistant, Oregon State University, obenchar@oregonstate.edu
[6] Executive Director of Aerospace Programs, Oregon State University, richard.wirz@oregonstate.edu

I. Introduction

Ground-based accelerated life testing is important to electric propulsion devices to qualify them for longevity in deep space missions [1-3]. However, long duration testing in simulated vacuums can produce back scattering contaminants from the beam target that affects EP performance by Hall thruster channel ingestion and deposition across all surfaces which lowers ionization efficiency [4, 5]. As a result, numerous experimental tests and theoretical simulations were created within the last 50 years to analyze the behavior of different graphite materials against incident ion collisions [6-10]. Multiple studies have been performed using xenon while investigations of krypton are limited [11, 12]. However, predictive engineering models (PEMs) are constantly improving to better mitigate the effects of backscattering for accelerated life tests [13, 14], and including phenomenon such as implantation and ejection of incident ions [15]. Figure 1 summarizes carbon backsputter rates for recent efforts [2,12], which will be used later for comparison with results discussed herein. Sabiston and Wirz [13], have used higher-fidelity simulations to further investigate the mechanisms and influence of material design on sputtering generation and transport. In addition, reduced order modeling of particle flow within a facility is being examined to reduce particle flux of both background gases and sputterants to the thruster face [16]. The objective of this study is to characterize the sputtering and deposition results of a Hall thruster facility test using krypton propellant with common facility materials.

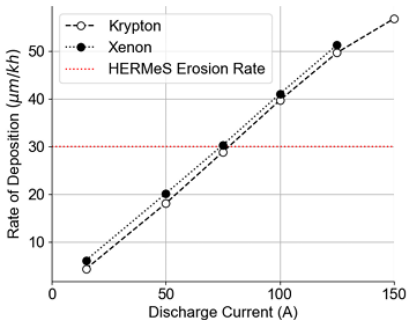

z_{target} (m)	Discharge Power (kW)	Theoretical Back-sputter (μm/kh)	Experimental Back-sputter (μm/kh)	Difference (%)
0.5	1.5	24.4	18.3	25.0%
0.5	3.0	48.8	44.6	8.6%
0.5	4.5	73.2	73.1	0.1%
0.5	6.0	97.6	96.5	1.1%
1.2	1.5	6.67	6.60	0.9%
1.2	3.0	13.3	13.4	-0.5%
1.2	4.5	20.0	20.2	-1.1%
1.2	6.0	26.7	26.7	-0.2%
1.2	9.0	40.0	44.5	-11.2%
5.3	6.0	1.45	0.91	36.7%
5.3	9.0	2.17	2.40	-10.7%
			Average |Diff.|:	**8.7%**

Fig. 1 (Left [10]) Carbon backscatter deposition due to 300 V Hall thruster operating on xenon and krypton. (Right [2]) Carbon backscatter data and theory for a xenon-fueled H6MS for 1.5 – 9.0 kW.

II. Sputtering Rate Estimation

To predict and average sputtering rate, $\dot{s}_{avg}$, we utilize a simple model developed by Biswas, et al. [11] which results in the following relationship:

$$\dot{s}_{avg} = \frac{m_s J_b P_b(\theta_s)}{2 d_t r_s} Y_0(V_a)$$

For the conditions reported in section III, we use this relationship for a thruster operating at J_b = 15 A and V_a = 300 V with a small witness plate placed d_t = 4.8 m downstream and off-center by r_s = 0.1 m. We use $\theta_s = \text{atan}\left(\frac{r_s}{d_t}\right)$ = 10.68°, amorphous carbon target material with Y_0(311 V) = 0.065 $\frac{\text{atoms}}{\text{ion}}$ (from [17]), an approximate target density of ρ_c = 1720 $\frac{\text{kg}}{\text{m}^3}$, and normalized beam current of $P_b(10.68°)$ = 1.95. The average erosion rate from Eq. 20 is

$$\dot{s}_{avg} = \frac{1.99x10^{-26}\ \text{kg}}{(1.6*10^{-19}\text{C})(1720\ \frac{\text{kg}}{\text{m}^3})} \frac{(15\ \text{A})(1.95)}{(4.8\ \text{m})(0.1\ \text{m})} 0.065 = 2.86 \frac{\mu\text{m}}{\text{kh}}$$

From Section III, for the "Baseline" condition for 20 hours, we expect 20 h * 2.86 $\frac{\mu\text{m}}{\text{kh}}$ = 0.057 μm of erosion on the target plate. Adding the 20 hours at "High Power" with yield Y_0(612 V) = 0.08 $\frac{\text{atoms}}{\text{ion}}$ [17], we anticipate an expected range from 0.1 μm to 1 μm for the total duration of both exposures, which is very small.

The 38th International Electric Propulsion Conference, P. Baudis Convention Center, Toulouse, France June 23-28, 2024

III. Deposition Estimation

To predict the deposition rate, we make an approximation for the internal surface area of Georgia Institute of Technology's LVF2 chamber which can be estimated from a cylindrical body with hemispherical ends. Here we will neglect the hemisphere where the thruster is located as an ideal case.

$$A_s = 2\pi rh + \pi r^2 \approx 165 \text{ m}^2$$

By assuming a density for carbon powder, we can estimate the deposition rate from a theoretical sputter yield of carbon [7] from our known thruster test conditions.

$$\dot{m}_C = \dot{m}_{prop} \left(\frac{m_C}{m_{Kr}}\right)\gamma \approx 423 \frac{\text{mg}}{\text{h}}$$

Lastly, we can find our deposition height by converting the mass flow into a volumetric flow rate of carbon and relating the quantity to the total surface area of the chamber.

$$\dot{V}_C = \left(423 \frac{\text{mg}}{\text{h}}\right)\frac{1}{\rho_C} \approx 6.3\, x\, 10^{-7} \frac{\text{m}^3}{\text{h}}$$

$$\frac{\dot{V}_C}{A_s} \approx 3.8 \frac{\mu\text{m}}{\text{kh}}$$

Thus, we expect the deposition inside of the chamber should be less than a micron, ~0.15 μm, after a 40 h test..

IV.H9 Hall Effect Thruster Experiment

A. Hall Thruster Test Operating Conditions

This test was performed at the Georgia Institute of Technology using the university's LVF2 vacuum facility from their High-Power Electric Propulsion Laboratory (HPEPL). The chamber facility walls are made from stainless-steel 304 with a polycrystalline-synthetic graphite [18] beam target that is located 4.8 meters from the thruster exit plane. Shown in figure 1 is a cross-sectional area and representation of the inner chamber beam target design where the numbered locations represent paneled surfaces that take in a fraction of the total fluence from the outlet as referenced from the model [13]: surfaces 29 through 34 and 39 through 41 are shrouds for the vacuum pumps. The diameter of the chamber is 4.87 meters, and the total length is 9.14 meters, not including the beam target geometry. Two different ignition tests were conducted: the thruster operated at 4.5 kW for 20 hours (baseline) and at 9 kW (high power) for 20 hours for a total of 40 hours of combined testing.

Table 1. H9 Hall effect thruster test conditions

Thruster Operating Condition	Duration [h]	Discharge Voltage [V]	Discharge Current [A]	Discharge Power [kW]	Anode Flow Rate [sccm]	Cathode Flow Rate [sccm]	Chamber Pressure [Torr]
Baseline	20	311	14.6	4.541	184	12.88	6×10^{-6}
High Power	20	612	14.8	9.054	188	13.16	6×10^{-6}

The 38th International Electric Propulsion Conference, P. Baudis Convention Center, Toulouse, France June 23-28, 2024

B. Target Plates

To assess chamber surface erosion due to beam impingements, target plates were placed directly in view of the H9 Hall effect thruster as shown in Figure 1. The approach was informed by insights from parallel [15] and previous [19, 20, and 21] sputtering research. Polycrystalline graphite targets were placed on panels 1, 2, and 42 as illustrated in figure 1. The two different types of graphite are graphite 060, denominated by its grain size of 0.06 in and graphite 030 with a grain size of 0.03 in. These 6.45 cm^2 square targets (0.635 cm in thickness) were etched with a orthogonal trenches roughly 100 µm deep to assist in locating surface features for microscopy before and after the testing. Identical locations were imaged with a Scanning Electron Microscope (SEM) at feature sizes down to the 5-um range for consistency.

Stainless steel 304 panels were also etched and imaged with an SEM and placed to the right of the thruster against the chamber wall to reflect locations 14 through 21 from Figure 1. Panel location along the wall varies by total ion flux and angle with respect to the thruster exit plane. The stainless-steel panel located on panel 21 is within the charge exchange (CEX) plume of the thruster [22].

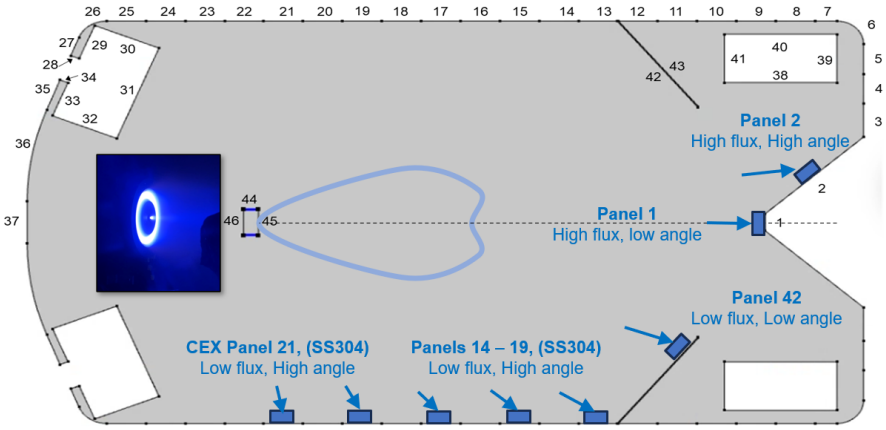

Figure 1. Target Plate Locations diagram inside the LVF2 Chamber for H9 Hall Thruster Ignition Testing

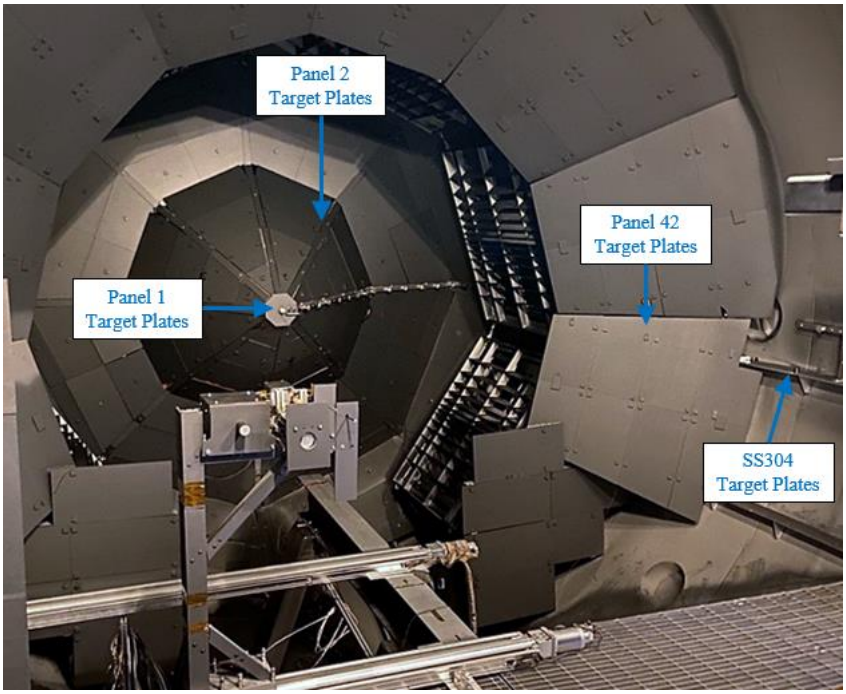

Figure 2. LVF2 Chamber Target Plate Locations corresponding to diagram

V. Results and Discussion

A. Results: Graphite Target Plates

As discussed before, we do not anticipate major feature changes for the target and witness plates. Therefore, a portable microscope was used to investigate the surface features of the graphite beam target for the LVF2 vacuum facility as conditions for steady-state surface morphology. According to HPEPL, the panels have not been replaced within the last 10 years and have been exposed to an untraceably large amount of incident ions from numerous commercial and research propulsion tests. Shown in Figure 3 are standard microscope images taken of the beam target surfaces that are macroscopically shown in Figure 2. Looking at the surface characteristics of the center panel (#1), the surface morphology appears to have random macroscopic characteristics that are not consistent with regular surface features (see Figure 5 [19], albeit for carbon-carbon) or surface flattening [23]. This implies that the steady-state surface morphology does not evolve to a regular or flat surface due to long-term ion irradiation but maintains macroscale features that should be considered for sputtering behavior predictions.

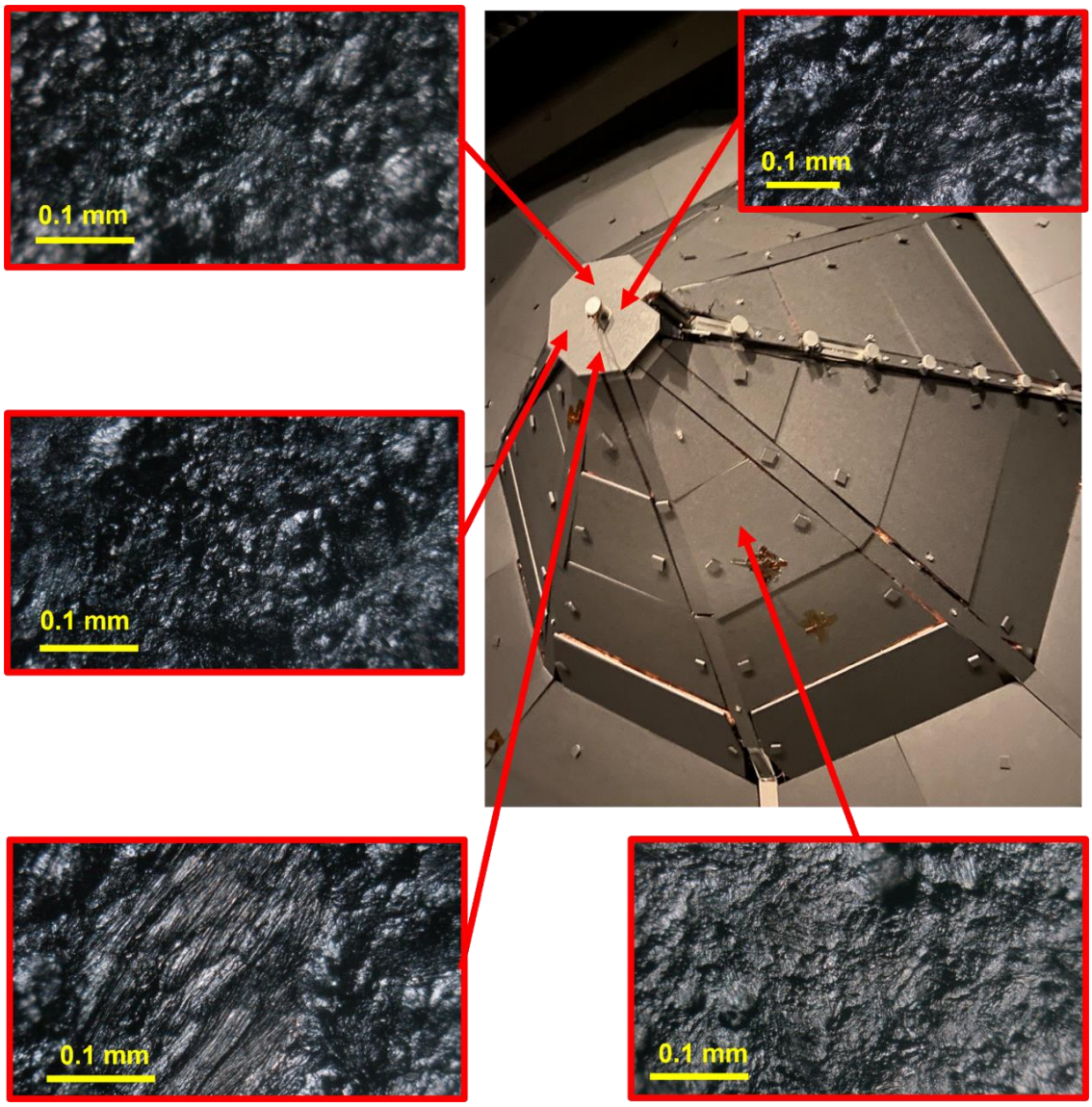

Figure 3. Beam Target Steady State Surface Features

SEM images were taken of the graphite target plates before and after the combined baseline and high-power tests for qualitative results from Table 1. Shown in Figure 4 is a comparison between the behavior of graphite 030 and graphite 060 after 40 hours of testing.

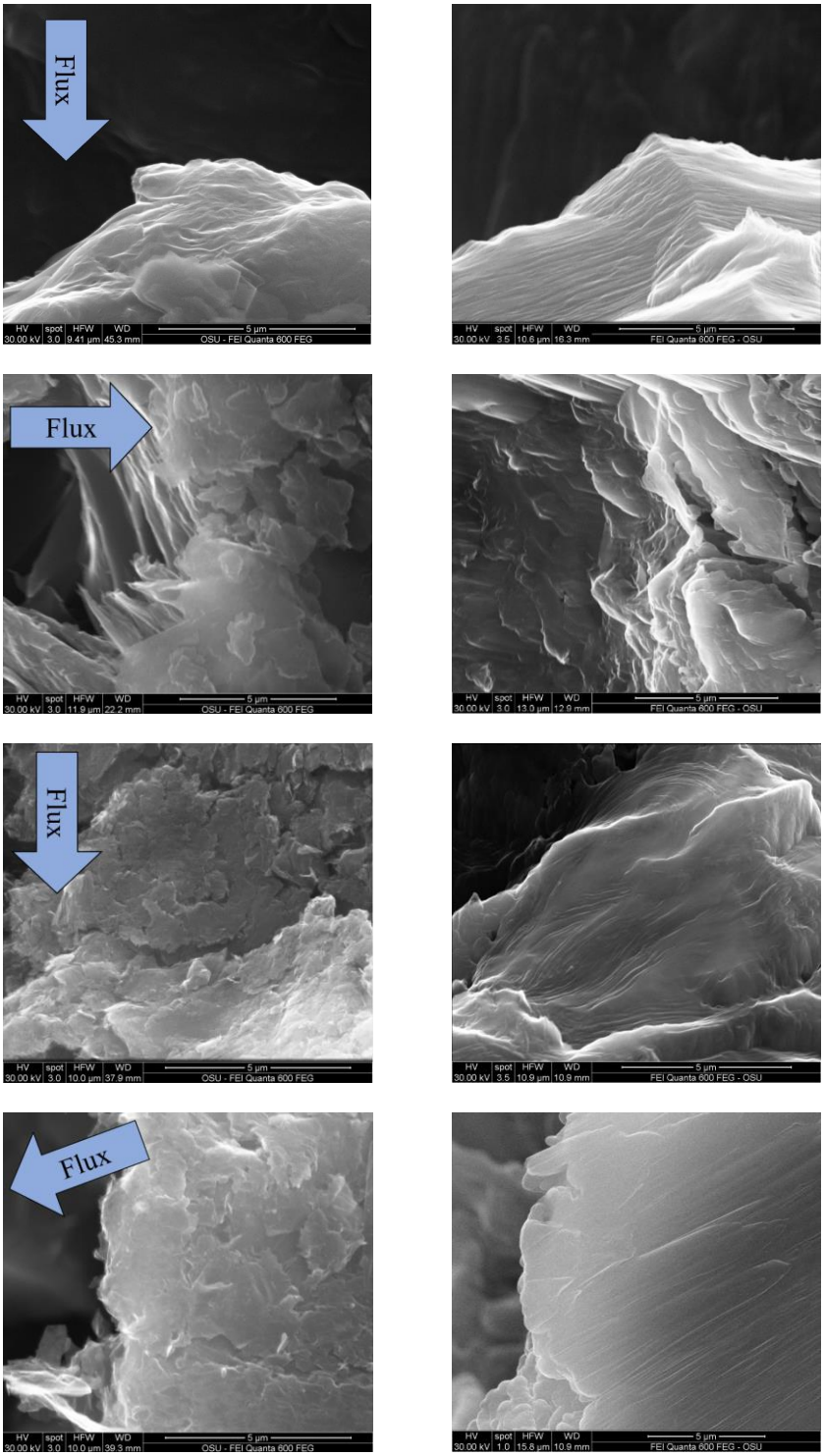

Figure 4. SEM of polycrystalline graphite at normal incidence (Panel 1) and high angle incidence (Panel 2) before (on the left) and after (on the right) 20 h of 4.5 kW and 20 h of 9 kW exposure.

After the 40-hour ignition test, smoothing of jagged edges into uniform ridges is visible for both panels 1 and 2 and is consistent with other forms of graphite erosion tests performed in literature. Deltschew et al. performed a similar test with xenon on carbon-carbon [19]. Shown below in Figure 5 is the evolution of a carbon-carbon composite before and after 4 hours of normal incident xenon ion bombardment. In comparison to the surfaces from the current test, it appears that the polycrystalline graphite does not exhibit similar patterning.

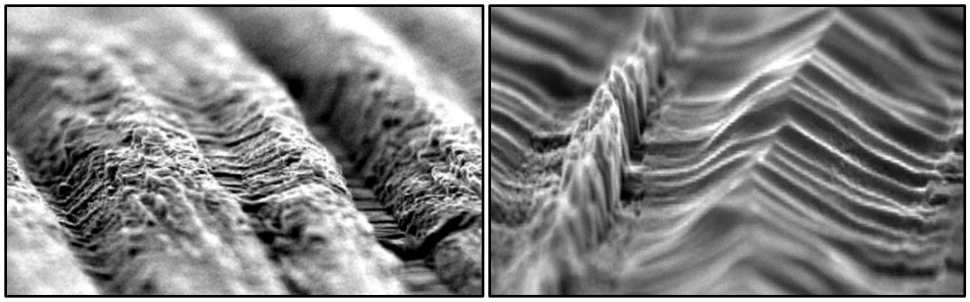

Figure 5. SEM of carbon-carbon composites with 500 eV Xenon Ion Energy [15]

The graphite manufacturers who made the HPEPL beam target panels said that the material is synthetic graphite which is made from petroleum coke and coal pitch tar [24]. The compound is extruded into the shape by baking at 1370 C and graphitized around 2500 C. This process is entirely separate from pyrolytic carbon which is made from thermal decomposition of hydrocarbons. Polycrystallinity for our target plates have been verified with an XRD (X-Ray Diffractometer) to compare against other polycrystalline graphite erosion and deposition tests [2].

Experimental sputter yield data is provided in Table 2 for graphite 030 samples that were masked and exposed to 10 hours at baseline conditions. Height measurements were made between the masked region as a reference point and the unmasked region to determine the total volume lost. Converting to a mass and dividing by the total fluence gathered from a Faraday probe is how our sputter yield is calculated. Current uncertainty is further discussed in section D.

Table 2. Graphite 030 Experimental Sputter Yield Data

GR030 Sample Location	Thruster Operating Condition	Duration [h]	Discharge Voltage [V]	Discharge Current [A]	Average ΔH [nm]	Experimental Sputter Yield	Sputter Yield Uncertainty
Panel 1	Baseline	10	311	14.6	666.323	0.08329	0.213
Panel 2	Baseline	10	311	14.6	974.490	0.206	0.207

B. Results: Stainless Steel Target Plates

After exposure from the H9 thruster test, pictures were taken of the stainless-steel beam targets. Shown below in Figure 6 is an example of one of the plates that was placed 82° from the thruster axis after testing.

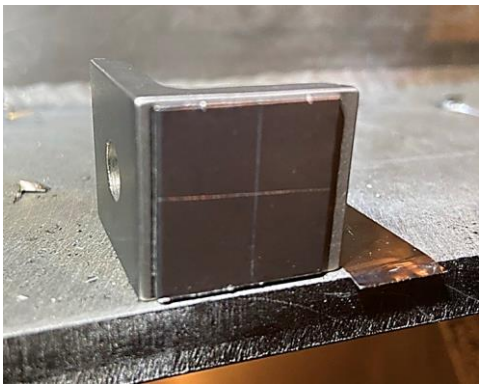

Figure 6. Stainless steel target plate after 20 hours at 4.5 kW and 20 hours of 9 kW.

For the 40-hour combined exposure, SEM images were taken before and after just like the graphite analysis. Shown below are images of stainless steel 304 panels along the side wall in Figure 7. Angle is recorded with respect to the thruster axis as well as scale measurements of how surface morphology is changing from high angle impinging krypton ions.

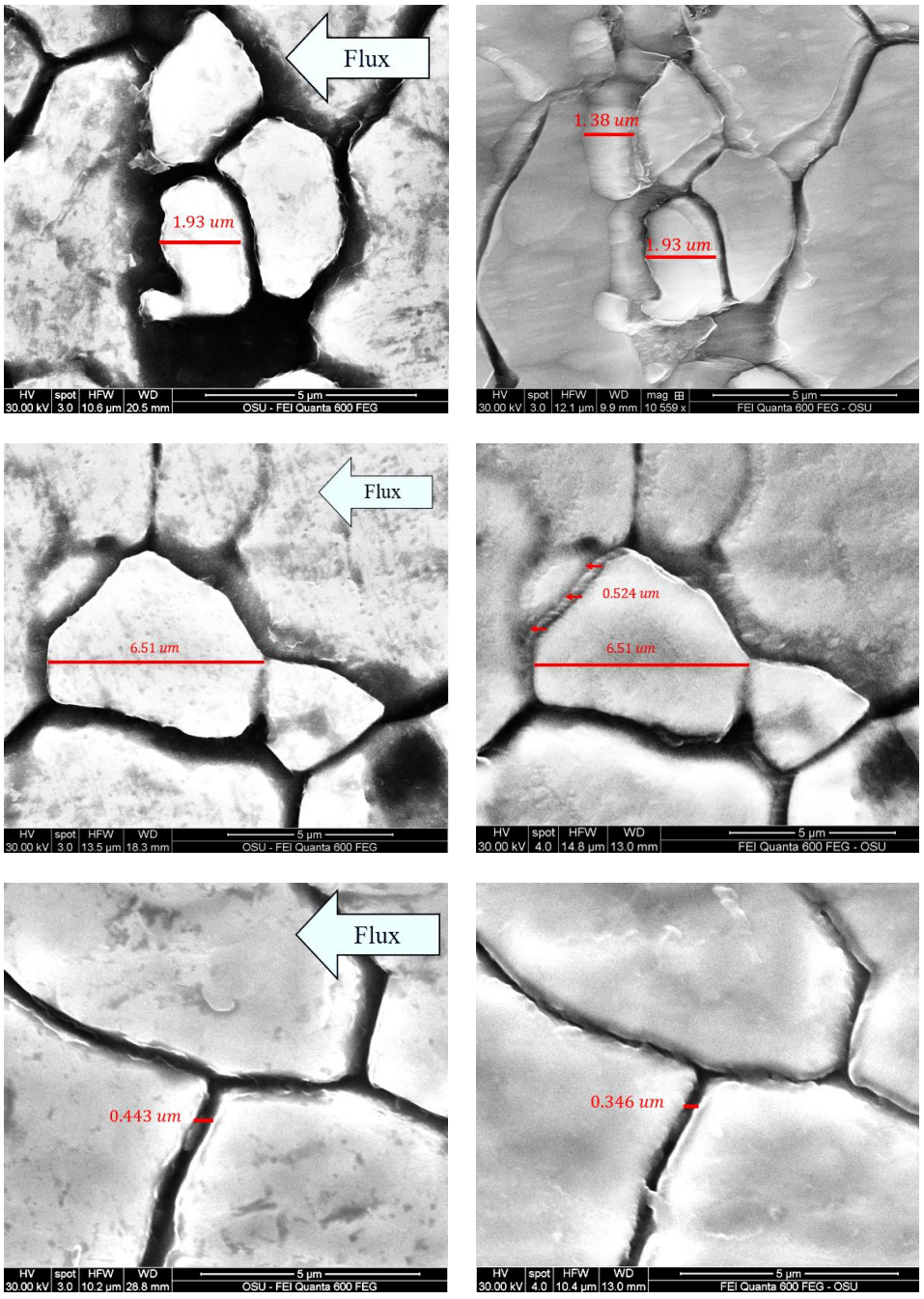

SS304
Panel 13
θ = 35 °

SS304
Panel 17
θ = 57 °

SS304
CEX Region
Panel 21
θ = 82 °

Figure 7. Stainless steel SEM image before (on the left) and after (on the right) 40 hours of exposure at various angles along the side wall of LVF2.

Pictures were taken of the side walls of LVF2 noting that flakes of material were present along the inner surfaces of the vacuum facility from previous tests beforehand as shown in Figure 8. These flakes were scraped off before the test began, but images of the side wall were taken with a portable microscope before doing so. Striations are visible along the walls of the chamber which have not been covered or repaired for all previous tests according to HPEPL.

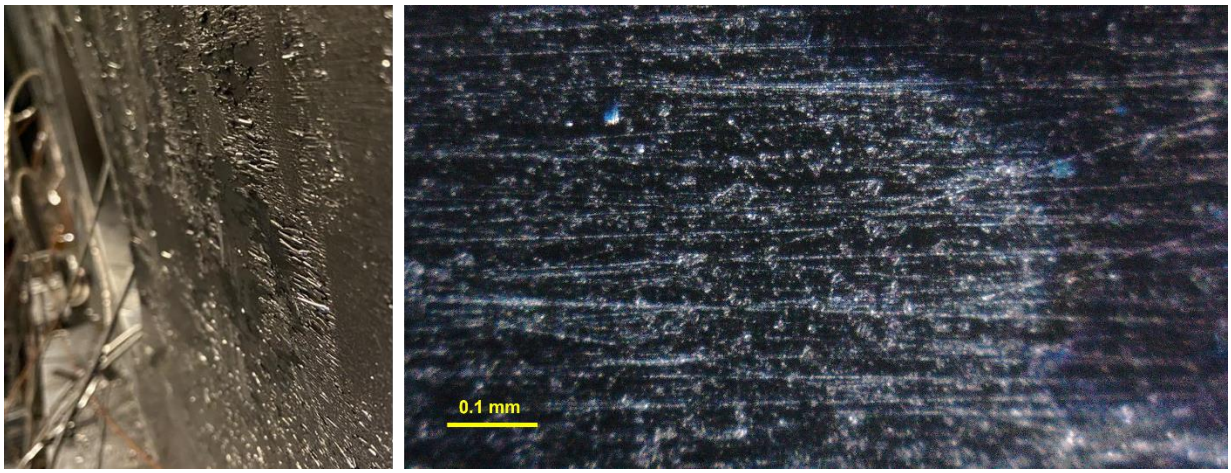

Figure 8. Stainless-steel chamber wall (on the left) and microscope features (on the right) on the chamber wall located by Panel 16.

C. Results: Witness Plates

Witness plates were placed as represented in Figure 9 to experimentally quantify deposition from the beam target. As shown in Figure 10, all witness plates are made of Indium Tin Oxide (ITO) coated glass and are 2.54 cm by 2.54 cm in area like the graphite and stainless-steel targe plates. The witness plates were not directly in view of the thruster to negate sputtering from primary incident ions, masked with non-coated quartz glass against the substrate, and wrapped with Kapton tape to avoid any constituents from interacting with the masked surface. Measurements were made using laser confocal profilometry with the Keyence VK-X3000 by comparing reference heights of the masked region to the unmasked total deposition area. Shown in the appendix is a table for 40 hours of exposure for deposition and height relative to distances away from panel 1 which is the center of the beam target.

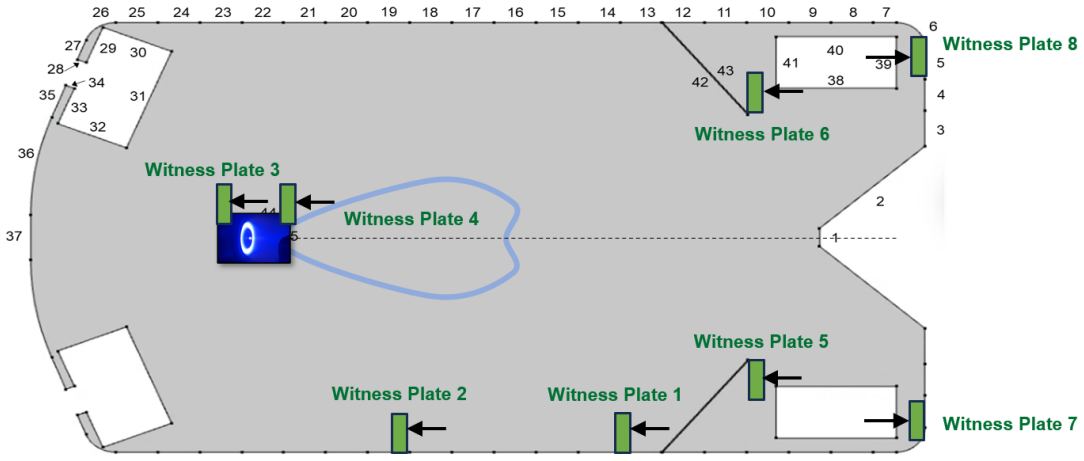

Figure 9. Witness plate location diagram for H9 Hall Thruster Testing

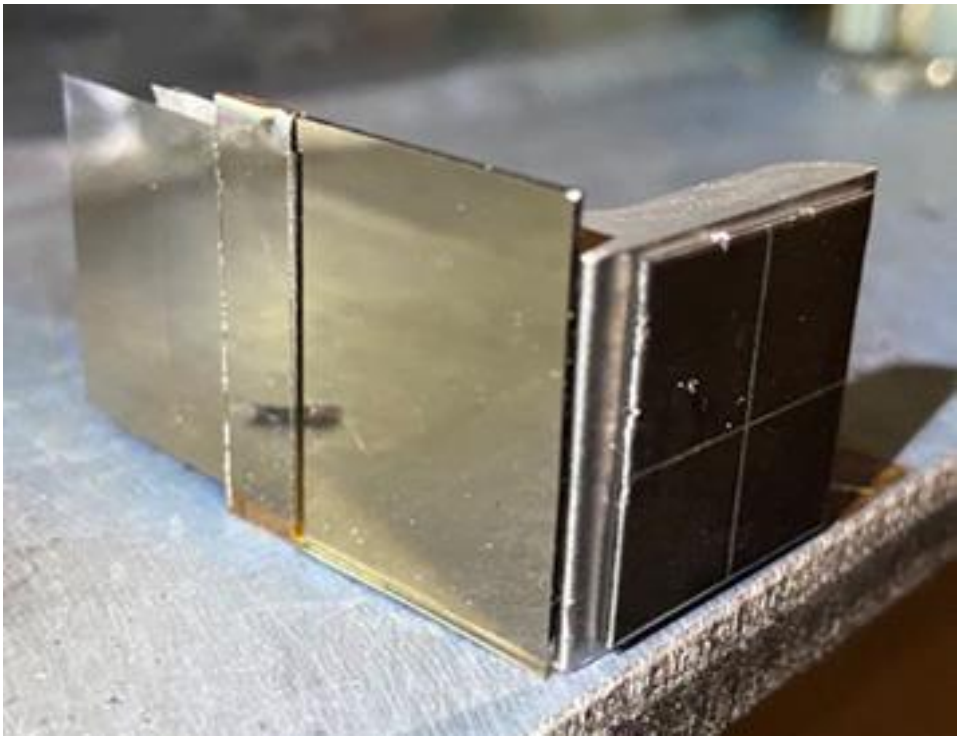

Figure 10. Masked ITO glass witness plate in the shadow of a stainless-steel target plate before testing

Table 3. Witness Plate Deposition Measurements for 40 hours of exposure for 20 hours at each 4.5 and 9 kW.

Witness Plate	Distance from Panel 1 (m)	Change in Height (um/kh)
1	3.11	7.97
2	4.95	2.96
3	4.78	Inconclusive*
4	5.43	5.11
5	1.61	Inconclusive*
6	1.61	8.78
7	2.07	8.53
8	2.07	11.2

D. Discussion

All erosion and deposition measurements are taken from calculating the arithmetic mean averages via laser confocal profilometry. This provides significant room for uncertainty depending on where the average measurements are taken. For the graphite beam targets, the average surface roughness is larger than the total erosion which means that low-pass and high-pass bands must be placed on the total scan which is not conducive when comparing the masked section versus the eroded substrate. More techniques need to be investigated to account for the higher surface roughness from GR060.Thruster misalignment provides uncertainty in the total fluence to each sample as well. The witness plates when placed under vacuum experience stress and strain that produces large height anomalies known as telephone cord buckling which can alter the height measurement by a relative angle [25]. Aside from buckling, they can also delaminate which will provide uncertainty in the original measurements. As a result, some of the witness plates potentially experienced erosion instead of deposition based on the scanned areas of the plates. In the appendix are all the original profilometry measurements in which the total erosion and deposition for the witness plates are shown.

Surface microscopy measurements were calibrated on site with a soft calibration card at a fixed distance between the target and lens for image consistency. However, due to macroscopic surface roughness of the beam target, only sections of each image remain in focus which provides uncertainty in the calibration. As a result, small changes in focus were necessary which will add uncertainty to the resulting feature scales.

Lastly, while total changes in height measurements were made, that does not provide sufficient analysis of the total constituents that are present. Preliminary Energy-dispersive X-ray spectroscopy (EDS) measurements were made on witness plate 4 which is closest to both the stainless-steel perforated floor and to the thruster in comparison to all other witness plates. While preliminary EDS results in Figure 11 show evidence of stainless-steel sputtered material is present on the witness plate, further analysis is required. Most notably, EDS penetrates the bulk of the material instead of only viewing surface quantities, thus additional approaches are being considered.

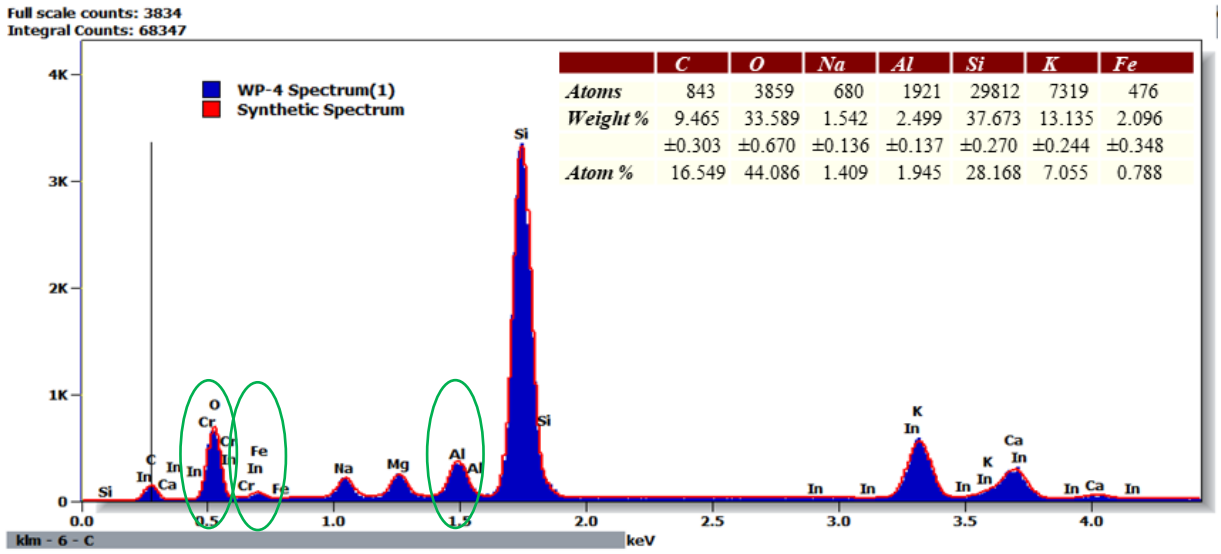

Figure 11. ITO glass witness plate 4 EDS test after 20 hours at 4.5 and 20 hours at 9 kW.

VI. Conclusion

A somewhat unexpected observation is that visualization of synthetic graphite panels that have experience long term exposure to ion beams in the LVF2 facility show structures that are irregular and not indicative of flat or periodic surfaces. Scanning Electron Microscope (SEM) images of 40-hr exposed target materials of 030 and 060 graphite shows feature changes that are larger than the scale of expected surface erosion. These results provide useful qualitative surface analysis but additional tests are needed to inform our erosion models and understanding. Preliminary optical profilometry and laser confocal methods show backscatter to witness plates consistent with expectations; however, these results have high uncertainty due to the short duration of the test and surface uncertainties, but inform approaches for future tests. Preliminary Energy-dispersive X-ray spectroscopy (EDS) measurements reveal evidence of stainless-steel and aluminum sputtered material amongst the carbon constituents. Future work will include further assessment of beam target materials, target plates, and witness plates, including analyses by techniques such as X-ray photoelectron spectroscopy (XPS) for more quantifiable results of sputtering vacuum facility materials.

VII. Acknowledgements

This work was supported by the Joint AdvaNced PropUlsion InStitute, 20-STRI-FULL-0004, NASA Grant Number 80NSSC21K1118 and in part through NASA and Oregon Space Grant Consortium, cooperative agreement 80NSSC20M0035n. We give a special thanks to Janice Cabrera who coordinated all of the universities involved. This test could not be performed without my colleagues who helped design and perform the experiment from the Wirz Research Group nor without the material science technical expertise from the Electron Microscopy Facility personnel at Oregon State University.

Appendix

The following tables are initial profilometry data of the witness plates. Current efforts are to quantify these data and determine uncertainty to provide surface-specific deposition rates.

Witness Plates 1 and 2

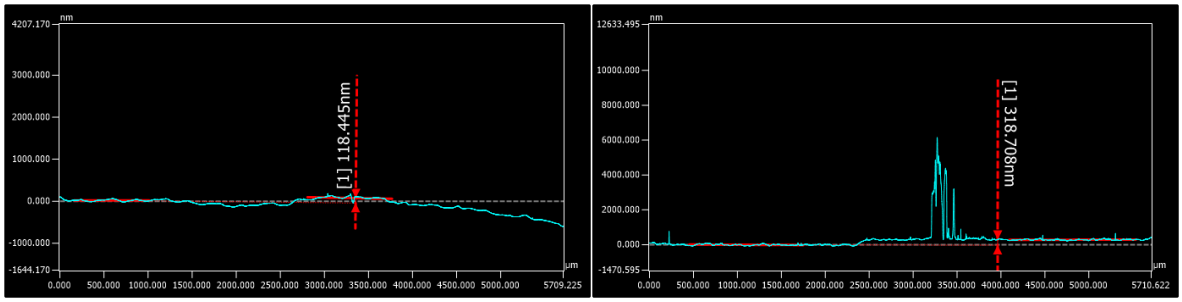

Witness Plates 3 and 4

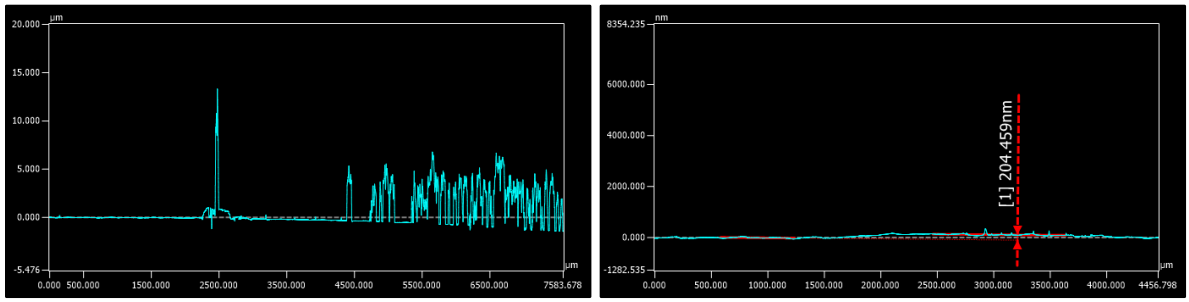

Witness Plates 5 and 6

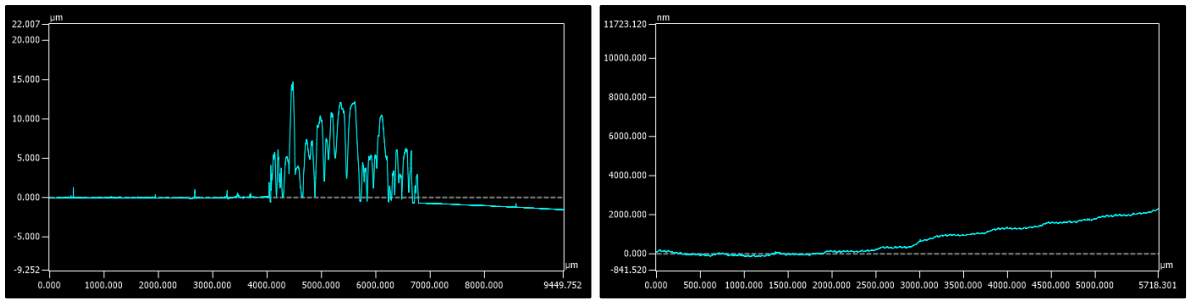

Witness Plates 7 and 8

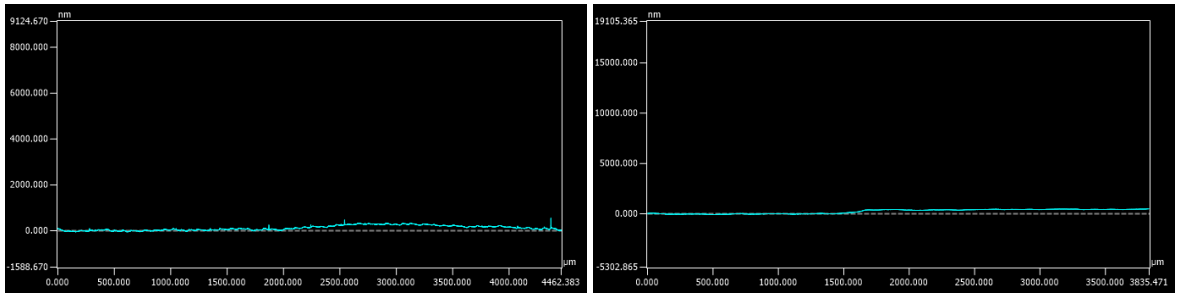

References

[1] Brophy, J. R., Polk, J. E., Randolph, T. M., and Dankanich, J. W., "Lifetime Qualification of Electric Thrusters for Deep Space Missions," AIAA 2008-5184, 44th AIAA/ASME/SAE/ASEE Joint Propulsion Conference, Hartford, CT, July 2008.

[2] Lobbia, R. B., Polk, J. E., Hofer, R. R., Chaplin, V. H., & Jorns, B. (2019). Accelerating 23,000 hours of ground test backsputtered carbon on a magnetically Shielded Hall thruster. *AIAA Propulsion and Energy 2019 Forum*. https://doi.org/10.2514/6.2019-3898

[3] Chris M. Cretel and Richard E. Wirz. Ion thruster grid life and performance assessment via reduced order modeling. In 38th International Electric Propulsion Conference, pages IEPC-2024-758, 2024

[4] Gilland, J. H., Williams, G., Burt, J. M., & Yim, J. (2016). Carbon back sputter modeling for hall thruster testing. *52nd AIAA/SAE/ASEE Joint Propulsion Conference*. https://doi.org/10.2514/6.2016-4941

[5] Duras, J., Kalentev, O., Matyash, K., & Schneider, R. (2013). Interactions Between Ion Thruster Plumes and Vessel Walls. *The 33rd International Electric Propulsion Conference*.

[6] Power, J. (1973). Sputter erosion and deposition in the discharge chamber of a small Mercury Ion Thruster. *10th Electric Propulsion Conference*. https://doi.org/10.2514/6.1973-1109

[7] Bohdansky, J. (1984). A universal relation for the sputtering yield of monatomic solids at normal ion incidence. *Nuclear Instruments and Methods in Physics Research Section B: Beam Interactions with Materials and Atoms*, *2*(1–3), 587–591. https://doi.org/10.1016/0168-583x(84)90271-4

[8] Yamamura, Y., & Shindo, S. (1984). An empirical formula for angular dependence of sputtering yields. *Radiation Effects*, *80*(1–2), 57–72. https://doi.org/10.1080/00337578408222489

[9] SOVEY, J., & PATTERSON, M. (1991). Ion beam sputtering in electric propulsion facilities. *27th Joint Propulsion Conference*. https://doi.org/10.2514/6.1991-2117

[10] Tartz, M., & Neumann, H. (2007). Sputter yields of carbon materials under xenon ion incidence. *Plasma Processes and Polymers*, *4*(S1). https://doi.org/10.1002/ppap.200731502

[11] Biswas, S., Cowan R. W., E. & Wirz. R. E. (2024) Hall thruster ion-induced sputtering of facility surfaces: Review of PMI data. 38th *IEPC International Electric Propulsion Conference*

[12] Su, L. L., Roberts, P. J., Gill, T., Hurley, W., Marks, T. A., Sercel, C. L., ... & Jorns, B. (2023). Operation and Performance of a Magnetically Shielded Hall Thruster at Ultrahigh Current Densities on Xenon and Krypton. In *AIAA SCITECH 2023 Forum* (p. 0842).

[13] Tran, H., & Chew, H. B. (2023). Surface morphology and carbon structure effects on sputtering: Bridging scales between molecular dynamics simulations and experiments. *Carbon*, *205*, 180–193. https://doi.org/10.1016/j.carbon.2023.01.015

[14] Sabiston, G., Wirz R. E. (2024) Electric Propulsion Vacuum Chamber Design Approaches for Reducing Sputtering Effects. 38th *IEPC International Electric Propulsion Conference*

[15] Luke K. Franz and Richard E. Wirz. Xe-C Scattering, Implantation, and Sputtering Analysis for EP Systems. In 38th International Electric Propulsion Conference, pages IEPC—2024—552, 2024

[16] Taghizadeh E., Obenchain R. A., Franz L. K., & Wirz. R. E. (2024) Electric Propulsion Facility Optimization via Reduced Order Modeling. In 38th International Electric Propulsion Conference, pages IEPC-2024-588, 2024

[17] Tran, H. D., Clark S. A., Thompson, R., Levin, De. A., Rovey, J. L., & Chew, H. B. (2024). Carbon Transport in Electric Propulsion Testing–I: Multiscale Computations for Carbon Sputtering by Low Energy Ion Bombardment. In *AIAA SCITECH 2024 Forum (P. 1135).*

[18] Tran, H., & Chew, H. B. (2024). Transient to steady-state morphology evolution of carbon surfaces under ion bombardment: Monte Carlo Simulations. *Acta Materialia*, *263*, 119498. https://doi.org/10.1016/j.actamat.2023.119498

[19] R. Deltschew, M. Tartz, V. Plicht, E. Hartmann, H. Neumann, Sputter Characteristics of Carbon-Carbon Compound Material. 27th International Electric Propulsion Conference, 2001

[20] Yalin, A. P., Williams, J. D., Surla, V., & Zoerb, K. A. (2007). Differential sputter yield profiles of molybdenum due to bombardment by low energy xenon ions at normal and oblique incidence. *Journal of Physics D: Applied Physics*, *40*(10), 3194–3202. https://doi.org/10.1088/0022-3727/40/10/025

[21] Williams, J., Johnson, M., & Williams, D. (2004). Differential sputtering behavior of pyrolytic graphite and carbon-carbon composite under Xenon bombardment. *40th AIAA/ASME/SAE/ASEE Joint Propulsion Conference and Exhibit*. https://doi.org/10.2514/6.2004-3788

[22] Wirz, R. E., Breddan, M. J. D., Konopliv, M., Obenchain, R. A., Cretel, C. M., Cowan, R. W., Franz, L. K., Haist, B., Biswas, S., Tisaev, M., & Parmar, S. (2024). Electric Propulsion Research Activities in the Plasma, Energy, & Space

[23] Li G., Wirz R.E., "Persistent Sputtering Yield Reduction in Plasma-Infused Foams," *Physical Review Letters*, 126 (3), 035001 (2021) https://doi.org/10.1103/PhysRevLett.126.035001

[24] Tamanshausky, A. V. (2006). An introduction to synthetic graphite. https://www.asbury.com/media/1225/syntheticgraphiteparti.pdf

[25] Volinsky, A. A., Waters, P., Kiely, J. D., & Johns, E. C. (2004). Sub-critical telephone cord delamination propagation and adhesion measurements. *MRS Proceedings*, *854*. https://doi.org/10.1557/proc-854-u9.5